Computational Modeling and Simulation of a Single-Jet Water Meter

Gorka S. Larraona
Alejandro Rivas
Juan Carlos Ramos

Thermal and Fluids Engineering Division,
Mechanical Engineering Department,
Tecnun (University of Navarra),
Manuel de Lardizábal 13,
20018 San Sebastián, Spain

A single-jet water meter was modeled and simulated within a wide measuring range that included flow rates in laminar, transitional, and turbulent flow regimes. The interaction between the turbine and the flow, on which the operating principle of this kind of meter is based, was studied in depth from the detailed information provided by simulations of the three dimensional flow within the meter. This interaction was resolved by means of a devised semi-implicit time-marching procedure in such a way that the speed and the position of the turbine were obtained as part of the solution. Results obtained regarding the turbine's mean rotation speed, measurement error, and pressure drop were validated through experimental measurements performed on a test rig. The role of mechanical friction on the performance of the meter at low flow rates was analyzed and interesting conclusions about its influence on the reduction of the turbine's rotation speed and on the related change in the measurement error were drawn. The mathematical model developed was capable of reproducing the performance of the meter throughout the majority of the measuring range, and thus was shown to be a very valuable tool for the analysis and improvement of the single-jet water meter studied. [DOI: 10.1115/1.2911679]

Keywords: single-jet water meter, CFD, fluid-structure interaction, measurement error, pressure drop, mechanical friction

1 Introduction

Single-jet meters are widely used for measuring water consumption in industrial, commercial, and residential applications. Their broad measuring range and remarkable low-flow sensibility, along with their long-term durability, make single-jet water meters a cost-effective choice for general billing purposes. Basically, they consist of a turbine contained in a chamber that rotates due to the torque imparted by a jet—formed as the flow enters the chamber—that impacts several of its vanes (Fig. 1). The speed at which the turbine rotates is expected to be proportional to the flow rate, so that the number of revolutions that the turbine turns is thereby proportional to the water volume delivered through the meter. The proportionality constant is usually known as the *meter factor* K (given in revolutions per volume unit) and it is determined for each meter design by experimental calibration.

However, the speed of the turbine is not exactly proportional to the flow rate and hence there exists a deviation between the volume registered by the meter—as K^{-1} times the number of revolutions given by the turbine—and the actual water volume delivered through it. This error in volume measurement depends on the flow rate and its variation throughout the measuring range of the meter is represented in the so-called *error curve* (Fig. 1). Manufacturers provide this curve together with the pressure drop curve, showing that the meter meets the requirements of the applicable standard (e.g., ISO, AWWA) regarding accuracy and maximum pressure drop.

Despite their simple operating principle, single-jet meters are difficult to theoretically analyze. On the one hand, the driving torque exerted by the jet depends on the position of the turbine, and it can hardly be quantified due to the complex interference that exists between the vanes impacted. On the other hand, the turbine is not likely to rotate with constant speed owing to the variable torque exerted by the jet, so it is also complicated to estimate the retarding torque produced upon the vanes of the turbine that are not impacted by the jet and which drag water. In addition, there is a nonhydraulic torque related to mechanical friction that acts against the rotation of the turbine. This torque is also difficult to quantify, although it is known to be significant only in the lower part of the measuring range [1], where it is responsible for the steep decline that is often observed in the error curve (see Fig. 1). In one of the few studies found in the bibliography, Chen [2] proposed a very simplified theoretical model for these forms of torque that assumes that the turbine rotates at a strictly constant speed for a given flow rate and that there is no interference between the vanes impacted by the jet. Moreover, it accepts that the torque on each vane is constant regardless of the position of the turbine and only depends on whether the vane is impacted by the jet or if it drags water. With these hypotheses and introducing an empirical constant to the model, he was able to reproduce the error curve of a specific design. However, the model is not capable of predicting the effect of the main design parameters on the performance of the meter, and therefore it cannot be employed for design purposes.

Due to the lack of a solid theoretical basis, the design and improvement of single-jet water meters have been mainly achieved so far by means of the experience gathered by each manufacturer in costly experimental procedures. This methodology involves building expensive prototypes and a large number of tests, which are limited to assessing the error and pressure drop curves of the new meter designs. Therefore, improvements in performance obtained with this methodology are often difficult to interpret and are not universally applicable.

Alternatively, computational fluid dynamics (CFD) techniques have been successfully employed for the study of several types of flow meters that, such as single-jet meters, have an operating principle based on the interaction between the flow and a moving element. Buckle et al. [3] studied the laminar flow around the float of a variable area flow meter and found reasonable agreement between the computed velocities and the Laser Doppler Anemometry (LDA) measurements they performed. They concluded [4]

Contributed by the Fluids Engineering Division of ASME for publication in the JOURNAL OF FLUIDS ENGINEERING. Manuscript received June 13, 2007; final manuscript received February 5, 2008; published online April 25, 2008. Assoc. Editor: Yu-Tai Lee.

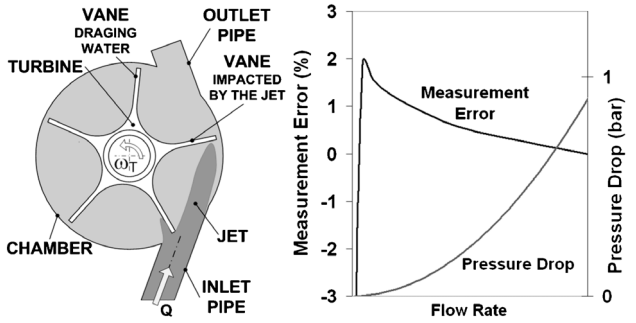

Fig. 1 Single-jet water meter: schematic of the operating principle (left) and typical error and pressure drop curves (right)

that the discrepancies were probably due to the asymmetry in the experimental flow. Xu [5] studied the flow around an isolated blade of an axial turbine flow meter and calculated the torque exerted by the flow on a radial section of the blade at different angles of attack and flow rates. These torques were later introduced in an analytical model of the flow meter [6] that also included all other torques applied to the turbine (e.g., bearing friction). The prediction of the error curve of the flow meter showed good agreement with the curve experimentally obtained. Aboury et al. [7] worked on an oscillating-piston water meter model. They used a deforming mesh and an implicit fluid-rigid body interaction algorithm and were able to quite accurately predict the error curve of the meter.

In the present study, the CFD based procedure described by Sánchez and Rivas [8] has been followed to develop a computational model for studying the performance of a single-jet water meter throughout a wide measuring range, which includes flow rates in laminar, transitional, and turbulent flow regimes. A semi-implicit time-marching procedure has been devised to resolve the complex interaction that exists between the flow and the turbine. This interaction has been studied in detail and the torques and turbine speed involved, which depend on the turbine position, have been calculated, so that valuable information for design purposes has been obtained. Results obtained regarding the turbine's mean rotation speed, measurement error, and pressure drop have been validated through experimental measurements performed on several units of the meter. The effect of mechanical friction on the lower part of the measuring range has been analyzed by considering different constant values of the associated retarding torque. The computational model is capable of reproducing the performance of the meter in this range when a specific amount of friction is considered.

2 Description of the Meter Studied

The meter studied (Fig. 2) is a noncommercial design that has been built following industry standards and can be considered as prototypical of a single-jet water meter for residential applications. Its five-vane turbine is contained in a cylindrical chamber that is enclosed by two ribbed plates above and below. The turbine is mounted on a pivot bearing and it has a magnet to transmit the number of revolutions by a magnetic coupling to the mechanical register located in a watertight enclosure. The gear ratio of the register is such that 1 litre is recorded whenever the turbine has turned 36.27 revolutions; thus the meter factor K is 36.27 rev/l. Both inlet and outlet pipes have straight ends that are aligned with the axis of the pipeline, but they are angled as they approach the chamber. In the case of the inlet pipe, the internal diameter is progressively reduced and the inlet strainer has been removed for simplicity.

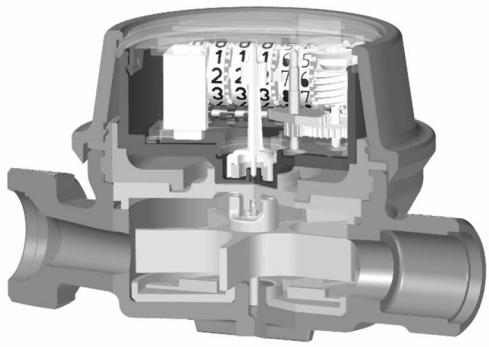

Fig. 2 Geometry of the single-jet water meter studied

Table 1 Summary of studied flow rates and corresponding pipeline Reynolds number and expected mean turbine speed ($\bar{\omega}_{T,\text{expected}} = 2\pi KQ/3600$, where Q is the flow rate in l/h)

Flow rate (1/h)	$\text{Re}_{\text{pipeline}}$	$\bar{\omega}_{T,\text{expected}}$ (rad/s)
15	352	0.95
22.5	528	1.42
30	704	1.90
60	1410	3.80
120	2820	7.60
300	7040	19.0
450	10,600	28.5
750	17,600	47.5
1500	35,200	95.0
3,000	70,400	190

The measuring range of single-jet water meters in residential applications usually expands from 15 l/h to 3000 l/h. Ten different flow rates within this range have been studied, so as to provide sufficient data to determine the overall performance of the meter. Table 1 shows the flow rates studied together with the corresponding Reynolds number based on the pipeline's internal diameter (15 mm) and the expected mean turbine speed, which is the result of the established meter factor. Taking into account the pipeline's Reynolds number, the flow within the meter is expected to be fully turbulent from 300 l/h. At lower flow rates, the flow might enter the meter in laminar regime and undergo a transition to turbulent regime inside. This transitional regime is more likely to happen in the case of 120 l/h and 60 l/h, even more so if the diameter reduction in the inlet pipe is taken into account. Because of this uncertainty about the possible transition to turbulence within the meter, simulations of flow rates up to 120 l/h have been performed considering the flow both in laminar and transitional regimes. Higher flow rates have only been simulated as fully turbulent.

3 Mathematical Model

Since the operating principle of the single-jet water meter is based on the interaction between the flow and the turbine, both water flow and turbine rotation have to be modeled and coupled in order to simulate the performance of the meter. The mathematical model developed considers the two-way coupling.

- Flow to turbine: The torque exerted by the flow is included in the differential equations that define the rotation of the turbine (Sec. 3.2). At each instant, the torque is computed and the speed and position of the turbine recalculated by integrating these equations.
- Turbine to flow: Time dependent position and speed of the turbine are included in the computation of the water flow. On the one hand, the domain in which the water flow is calculated is variable in time and accommodates the position of the turbine at each instant (Sec. 3.1). On the other hand, the velocities of water particles in contact with the

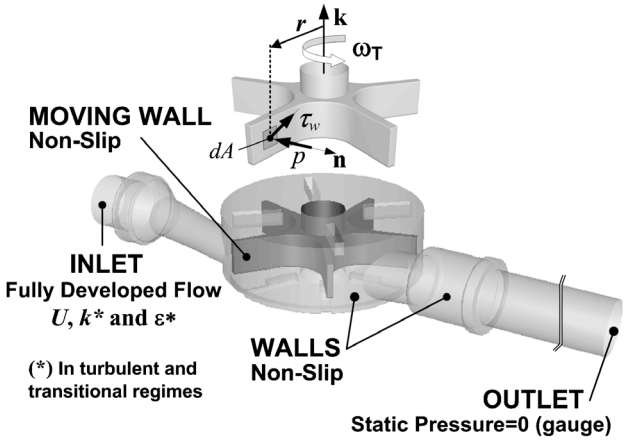

Fig. 3 Flow domain and boundary conditions. (Pressure and shear forces exerted by the flow on the turbine are also depicted.)

turbine are set at each instant to those of the turbine points by the nonslip boundary condition (Sec. 3.3).

As a result of solving the interaction between the turbine and the water flow, the variations of both the torque exerted by the flow and the rotation speed of the turbine will be obtained. They are expected to periodically vary since the five-vane turbine recovers the same position each 72 deg ($2\pi/5$ rad).

3.1 Flow Domain. The flow domain (Fig. 3) is defined as the volume delimited by the internal geometry of the meter, the turbine, and two sections of the pipeline to which the meter is threaded in its normal installation. As explained before, the flow domain is variable in time because the turbine rotates and occupies a different position at each instant. The pipeline has an internal diameter of 15 mm, and its sections before and after the meter are 15 mm and 90 mm long, respectively; these sections are considered long enough for the boundary conditions prescribed at their ends to be realistic (see Sec. 3.3).

3.2 Governing Equations

Water Flow. The flow within the meter is considered incompressible. Different forms of the Navier–Stokes equations are used depending on whether the flow rate simulated is considered as being in a laminar, transitional, or fully turbulent regime. When the flow is considered laminar, the unsteady Navier–Stokes equations are employed, which in vector form can be written as

$$\nabla \cdot \mathbf{u} = 0 \tag{1}$$

$$\frac{\partial \mathbf{u}}{\partial t} + \nabla \cdot (\mathbf{u}\mathbf{u}) = -\frac{1}{\rho}\nabla p + \nabla \cdot [\nu(\nabla \mathbf{u} + \nabla \mathbf{u}^T)] \tag{2}$$

On the other hand, the unsteady Reynolds averaged Navier–Stokes (URANS) equations are used when the flow is considered transitional or fully turbulent. Since the Boussinesq hypothesis [9] is adopted, these equations are as follows:

$$\nabla \cdot \mathbf{U} = 0 \tag{3}$$

$$\frac{\partial \mathbf{U}}{\partial t} + \nabla \cdot (\mathbf{U}\mathbf{U}) = -\frac{1}{\rho}\nabla P + \nabla \cdot \left\{ (\nu + \nu_t)[\nabla \mathbf{U} + \nabla \mathbf{U}^T] - \frac{2}{3}k\mathbf{I} \right\} \tag{4}$$

In these equations, the magnitudes that appear in capitals refer to ensemble averaged values; ν_t and k stand for kinematic eddy viscosity and turbulence kinetic energy, respectively, and they have to be calculated using a turbulence model. The two-layer approach of Chen and Patel [10] has been used for this aim, combining the two-equation realizable k-ε model [11] with the one-equation model of Wolfshtein [12], which is more suitable for reproducing viscous effects close to solid walls. Both models solve the same transport equation for k but calculate ε and ν_t in a different way. A smooth merging between the results of the two models is achieved by means of the blending functions proposed by Jongen and Marx [13].

The computation of transitional flows is currently an active topic of research. Customary turbulence models fail even in the prediction of the simplest case, so some specific models or modifications to the usual models have been proposed for the different types of transition [14,15]. Neither the realizable k-ε model nor the Wolfshtein model is suitable for accurately predicting the onset of transition from laminar to turbulent regime, although the latter can be tuned for transitional boundary layer calculations as explained by Rodi [16]. Therefore, simulations of the lower flow rates in transitional regime cannot be expected to reproduce turbulent quantities, such as ν_t and k, accurately. However, the impact of this restraint on the prediction of the integral quantities of interest, such as the rotation speed of the turbine, can be expected to be limited. The latter will be assessed comparing the results obtained with experimental measurements.

Turbine Rotation. Considering the turbine as a rigid body, its rotation is governed by the following system of ordinary differential equations:

$$I_T \frac{d\omega_T}{dt} = T_F - T_{\mathrm{PB}} - T_R \tag{5a}$$

$$\frac{d\varphi_T}{dt} = \omega_T \tag{5b}$$

where I_T is the turbine's inertia moment, ω_T and φ_T are its rotation speed and angular position, and T_F, T_{PB}, and T_R are the torques produced by the flow about the axis of the turbine, the pivot bearing, and the registration system, respectively.

The torque imparted by the flow (T_F) is the sum of the driving torque due to the impact of the jet on some of the vanes and the retarding torque due to the fact that the rest of the turbine drags water. Its magnitude depends on both the position and the speed of the turbine and it increases with the flow rate since both the momentum flux of the jet and the speed with which the turbine drags water become greater. This torque is calculated at each time step by integrating the torque of the pressure and shear forces about the rotation axis ($\mathbf{k}$) along the surface of the turbine (A_T) (see Fig. 3):

$$T_F = \left[\int\int_{A_T} \mathbf{r} \wedge (-p\mathbf{n} + \boldsymbol{\tau}_\mathbf{w}) dA \right] \cdot \mathbf{k} \tag{6}$$

On the other hand, the torques produced by the pivot bearing (T_{PB}) and the registration system (T_R) are owing to mechanical friction and always oppose the turning of the turbine, thereby slowing it down. The former is due to the contact that exists between the turbine and the pivot bearing around which it rotates. The latter is the torque needed to overcome the friction between the gears of the mechanical register and is transmitted to the turbine by the magnetic coupling. These two torques are not easy to model and will be combined into a single term: *mechanical resistance torque* (T_{MR}), which encompasses the effect of mechanical friction overall. Since the effect of mechanical friction has been reported to be of importance only in the lower part of the measuring range [1,17], mechanical resistance torque can be expected to be significant compared to the torque exerted by the flow only at low flow rates, where this torque is rather small. Because of the uncertainty about the magnitude that the mechanical resistance torque may have, different possible values will be considered in

Table 2 Numerical schemes used in simulations

Transport equation terms	Numerical scheme	Refs.
Unsteady	Second order	
Diffusive	Second order centered	
Convective	Second order upwind	[21]
Source	Midpoint rule integration	
Pressure-correction algorithm	SIMPLEC	[22]
Velocity interpolation in continuity equation	Rhie-Chow	[23]

the simulations of flow rates up to 120 l/h. This torque will not be regarded, however, in the simulations of higher flow rates.

3.3 Boundary Conditions. Boundary conditions for the water flow are applied at the walls of the meter and the pipes, at the surface of the turbine, and at the ends of the pipe sections (Fig. 3). In the case of the walls and the surface of the turbine, the nonslip velocity condition is imposed so that the fluid has the same velocity as the wall. In the simulations in transitional and turbulent regimes, they have been considered as smooth walls for shear stress calculation.

At the inlet, profiles corresponding to fully developed flow are prescribed for the velocity and—in the case of flows in turbulent regime—for the turbulence kinetic energy (k), and its dissipation rate (ε). In simulations in transitional regime, the velocity profile is that of the fully developed laminar flow and k and ε are set at very small constant values that make the turbulent viscosity ratio (ν_t/ν) of the order of 10^{-5}. Fully developed flow profiles have been obtained by means of a separate simulation of the corresponding flow rate in an infinite 15 mm diameter pipe, following the method described by Murthy and Mathur [18].

At the outlet, only the value of the static pressure is specified; the remaining flow variables are extrapolated from within the flow domain itself. The value given is zero gauge pressure. Since the flow has been modeled as being incompressible, only pressure gradients are significant, so any other constant value prescribed would lead exactly to the same result but with a shift in the pressure field of this constant value. The election of zero gauge pressure helps minimize the round-off error in the calculations [19].

Initial conditions are also to be equally provided for the flow variables and for the position and speed of the turbine. They are described below where the full process of initialization is explained (Sec. 4.2).

4 Numerical Simulation of the Mathematical Model

The unstructured CFD code FLUENT V.6.3 has been used to numerically solve the mathematical model. The time-marching procedure used for resolving the interaction between the turbine and the flow has been implemented with the help of the user defined functions of the code. FLUENT uses the finite volume method [19] to discretize the flow-governing equations with a collocated variable arrangement. The equations are integrated in each mesh cell and the resulting integrals approximated using a multidimensional linear reconstruction approach [20]. Numerical schemes used in the simulations are listed in Table 2.

4.1 Flow Domain and Time Discretization. The flow domain has been discretized by means of an 815,000 hexahedral element mesh (Fig. 4). A cylindrical sliding mesh zone has been defined, which rotates together with the turbine while it slides past the mesh of the rest of the domain. Consequently, the discretized flow-governing equations are modified within this sliding mesh zone to account for the velocity of the cell faces. The nonconformal interface that exists between the rotating and the static mesh zones is treated employing the method described by Mathur [24], which avoids the need for interpolation and preserves the order of the numerical schemes at the interface.

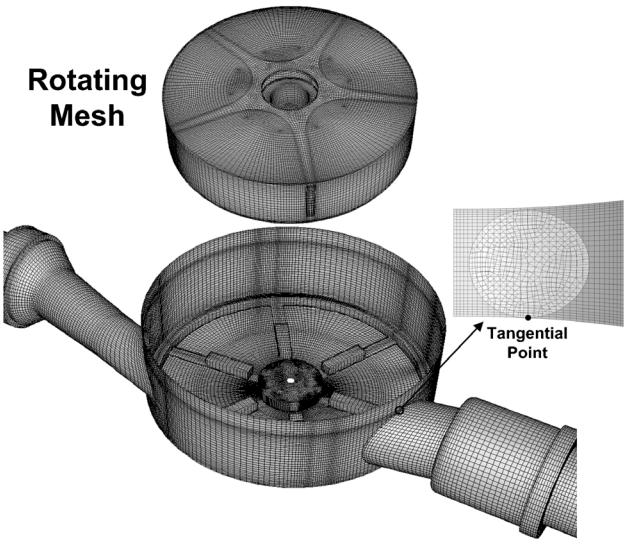

Fig. 4 Computational mesh with details of the moving mesh zone and the nonconformal mesh connecting the chamber and the outlet pipe

A nonconformal interface has also been used at the intersection of the chamber and the outlet pipe because there is a tangential point between them that would otherwise make the mesh of very poor quality. This procedure was not necessary at the intersection of the inlet pipe and the chamber since there is no tangency; there the mesh is fully conformal. Mesh points have been clustered near the walls of the chamber and the turbine to correctly resolve the boundary layers involved in the turbine-flow interaction. However, since boundary layers become thinner as the flow rate increases, a worse resolution of the boundary layers and larger values of y^+ at wall-adjacent cells have to be anticipated in the case of the highest flow rates.

The time step size (Δt) has been set for each simulation so that approximately 1200 integration steps (N_{steps}) are given in each revolution of the turbine (Eq. (7)). Specifically, it has been $\Delta t = 5 \times 10^{-3}$ s in the simulation with a flow rate of 15 l/h and $\Delta t = 2.5 \times 10^{-5}$ s in the simulation with 3000 l/h. With the time step size so calculated, the turbine turns $\Delta\varphi_T \approx 0.3$ deg on average between two consecutive time steps. This angle of rotation is fairly smaller than the angle that Benra [25] recommended for a realistic unsteady simulation of the flow within a pump, and thus it is judged to be small enough to provide accurate results in this particular case.

$$\Delta t = \frac{2\pi}{N_{\text{steps}} \bar{\omega}_{T,\text{expected}}} \tag{7}$$

4.2 Initialization of the Simulations. A steady solution was first obtained prior to each simulation with the turbine set at a specific motionless position. The transient simulation was then initiated with the values of the flow variables obtained and the rotation speed of the turbine being progressively increased until the value expected for the corresponding flow rate was reached (see Table 1). Five time steps with linearly increasing speed were enough to reach the desired value in all cases. The rotation speed was maintained constant until the flow became almost periodic after the turbine had completed two turns. Thereafter, the speed and the position of the turbine were calculated at each time step following the time-marching procedure described below.

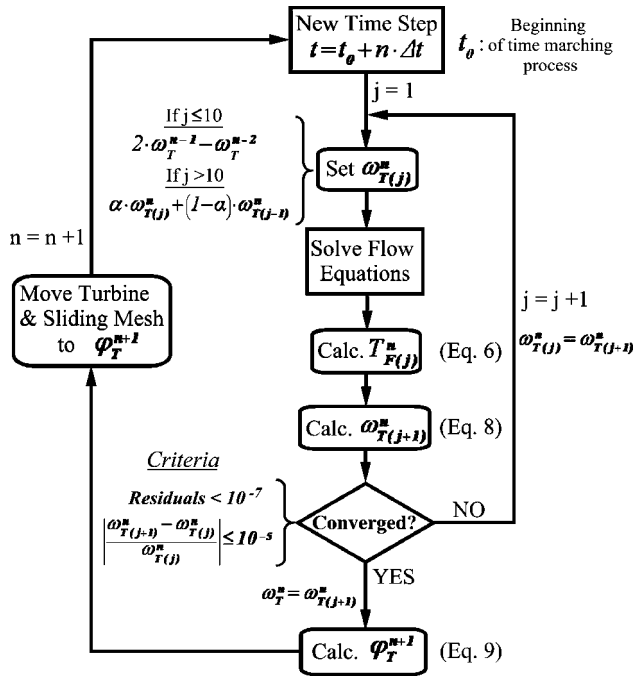

Fig. 5 Flow diagram of the semi-implicit time-marching procedure devised to handle turbine-flow interaction

4.3 Numerical Procedure to Handle Turbine-Flow Interaction. A semi-implicit time-marching procedure has been devised to deal with turbine-flow interaction (Fig. 5). Actually, the inertia moment of the turbine is very low and its rotation speed has shown to be very sensitive to the torque exerted by the flow. This makes the required time step size extremely small in order for the explicit time marching to be stable. The proposed time-marching procedure implicitly treats the turbine's rotation speed to overcome this restriction. The position, however, is explicitly treated. The procedure follows the steps described below:

(1) The rotation speed of the turbine is set at the beginning of each iteration step (j). In the first ten steps ($j\leqslant 10$), the rotation speed is maintained constant with the value obtained by linear extrapolation of the speeds at the last two time steps. From then on ($j>10$), the rotation speed calculated in the previous iteration step (see Eq. (8)) is underrelaxed and imposed on the turbine. A relaxation factor of $\alpha=0.3$ has been used.

(2) Once the rotation speed of the turbine has been established, the flow-governing equations are solved by means of the pressure-correction algorithm SIMPLEC, using an implicit point Gauss–Seidel method accelerated by an algebraic multigrid strategy.

(3) Next, the torque exerted by the flow is calculated with the values of velocity and pressure just obtained. This value is then used to compute the rotation speed for the next iteration step by integrating Eq. (5*a*) with the second order scheme:

$$\omega_{T(j+1)}^n=\frac{4}{3}\omega_T^{n-1}-\frac{1}{3}\omega_T^{n-2}+\frac{2}{3}\frac{\Delta t}{I_T}(T_{F(j)}^n-T_{\mathrm{MR}}) \qquad (8)$$

When mechanical resistance torque (T_{MR}) is considered, i.e., in flow rates up to 120 l/h, it is regarded as independent of the rotation speed, so it is not recomputed in each iteration step.

(4) Convergence is judged by checking (i) that the scaled residuals of the flow-governing equations in the iterative process are below 10^{-7} and (ii) that the variation of the rotation speed in two consecutive iteration steps is less than a 0.001%. Both requirements are usually met after 25 iteration steps.

(5) Once convergence is achieved, the rotation speed of the turbine is set to the last value calculated and its position in the next time step is calculated with Eq. (9). The sliding mesh is then moved to the new position and a new time step begins.

$$\varphi_T^{n+1}=\frac{4}{3}\varphi_T^n-\frac{1}{3}\varphi_T^{n-1}+\frac{2}{3}\Delta t\omega_T^n \qquad (9)$$

This procedure has two important advantages. First, the sliding mesh is only moved at the end of the time step, once the iteration process has been converged. The fully implicit approach, as that proposed by Aboury et al. [7], requires the readjustment of the position of the turbine within the iterative process of each time step, which makes the calculation more costly. Second, the implicit treatment of the turbine's speed guarantees that energy conservation in the fluid-solid interface is accomplished. As noted by Le Tellec and Mouro [26], this characteristic is essential both for preserving stability and ensuring the long-term accuracy of the numerical computation.

4.4 Convergence and Verification of the Simulations. Once the time-marching procedure is started it, nearly takes three complete revolutions of the turbine for each simulation to reach a periodic flow solution. Thereafter, the torque exerted by the flow and the rotation speed of the turbine repeat each time period T, which is the time needed for the turbine to complete 72 deg and recover the same position. However, in the case of flow rates ranging from 30 l/h to 120 l/h, the simulations performed assuming a laminar flow regime did not reach a periodic flow solution. Indeed, the nonperiodicity was more marked as the flow rate increases. This fact has been judged as an indicator that the flow is actually in transitional regime at these flow rates, and therefore, only the periodic torque and speed results obtained in this regime have been considered. On the other hand, simulations with 15 l/h and 22.5 l/h performed considering a laminar flow regime did reach a periodic flow solution. This fact would confirm that the flow is actually laminar at these two flow rates. Consequently, the results obtained from these simulations have been considered instead of those obtained assuming a transitional flow regime. In any case, the results obtained in both regimes showed minimum differences with regard to the torque exerted by the flow and the turbine's rotation speed.

The simulations have been considered as converged once the mean rotation speed of the turbine does not change more than 0.01% from period to period. A runtime of nearly 900 h in a PC with a 2.8 GHz Intel processor was typically necessary to attain this level of convergence. As will be shown below, the variation of the torque exerted by the flow and the turbine's rotation speed in each period is quite smooth, so the numerical dispersion related to time integration is believed to be rather low.

All simulations have been repeated in a coarser mesh of 410,000 elements in order to estimate the discretization error. This mesh has been obtained applying a coarsening factor of 1.25 in each coordinate direction of the original mesh. Accordingly, the time step size used in the simulations has been 1.25 times larger. The discretization error corresponding to the mean rotation speed of the turbine has been estimated by the *extrapolated relative error* proposed by Celik and Karatekin [27], using the formal order of accuracy of the numerical schemes employed. The estimated discretization error is below 1% in the case of the simulations up to 300 l/h. It is higher in the simulations of flow rates between 450 l/h and 3000 l/h, but it is still small, the highest errors estimated being those of 1500 l/h and 3000 l/h, which are 2.3% and 1.7% respectively.

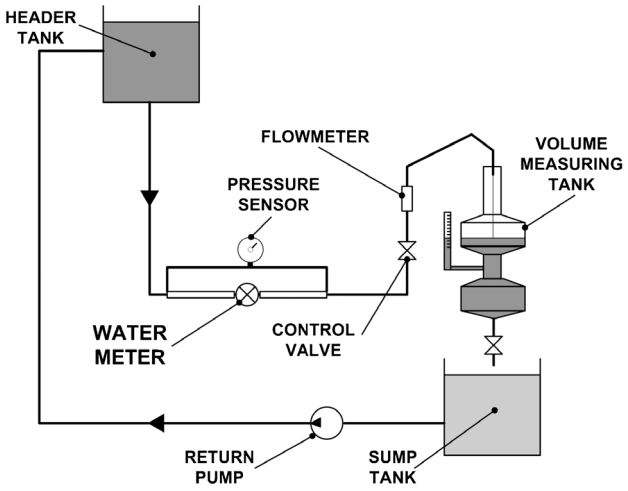

Fig. 6 Schematic of the experimental test rig

5 Experimental Measurements for Model Validation

Experimental measurements have been carried out in a calibration facility (Fig. 6). It includes a constant head tank that allows a steady water flow to pass through the meter by gravity, a series of control valves and variable area flow meters to establish the desired flow rate and a volume measuring tank into which the water is discharged. The meter is threaded to a horizontal pipe with an internal diameter of 15 mm. The pipe section before the meter is 250 mm long and is in turn preceded by a large radius bend; hence, the flow is expected to be fully developed when it enters the meter.

Three units of the meter have been constructed and tested in order to obtain the error curve, the mean rotation speed of the turbine, and the pressure drop. The results for each flow rate have been obtained by averaging the measurements of the three runs carried out with each unit. The dispersion of the data obtained in different runs and different units was rather small. The difference was less than 0.2% between data from the same unit and nearly 0.7% between data from different units.

Error in volume measurement is determined allowing a certain amount of water to pass through the meter and comparing the volume registered by the meter with the actual volume that is ascertained in the measuring tank. In the case of flow rates between 15 l/h and 120 l/h, a 10 l tank is used, whereas in the case of higher flow rates, a 100 l tank is utilized. Both tanks have a calibrated sight glass for reading water volume in their upper part. The time needed for total water volume to pass through the meter was also measured in each experiment and it helped assess the flow rate indicated by the flow meter by dividing the actual volume that had passed through the meter by the elapsed time. The error curve of the meter has been obtained performing measurements of the ten flow rates studied. The overall uncertainty in the error has been calculated to be $\pm 0.3\%$.

Mean rotation speed of the turbine for a given flow rate is inferred from the indication of the meter's register. The number of revolutions given by the turbine in an experiment is calculated multiplying the registered volume by the meter factor K. The mean rotation speed is then obtained dividing the number of revolutions by the time elapsed in the experiment.

Finally, pressure drop is measured in the case of the highest flow rates, namely, 450 l/h, 750 l/h, 1500 l/h, and 3000 l/h, using a differential pressure sensor connected to two pressure tapings that are located 200 mm before and 150 mm after the water meter, respectively. The pressure sensor has an uncertainty of $\pm 1\%$ of the full-scale reading, which is 2 bars. Pressure losses provoked by the pipe sections that are not included in the mathematical model have been estimated and subtracted from the measurements. The pipes have a very low roughness and have been considered as being hydraulically smooth, so their friction factor has been calculated using the Blasius formula [28]. The subtracted pressure losses represent about 4% of the measured value at all four flow rates.

6 Results and Discussion

6.1 Study of the Turbine-Flow Interaction. The numerical simulation of the flow within the single-jet water meter with different flow rates has allowed a detailed analysis of the interaction between the flow and the turbine. For example, Figs. 7–9 show some of the results obtained in the simulation of a flow rate of 3000 l/h. For this study, the initial position of the turbine ($\varphi_T = 0$ deg) has been arbitrarily defined as that in which one of the vanes impacted by the jet is perpendicular to the pipeline axis. Additionally, the side of each vane that is directly impacted by the jet when both come into contact is designated as the front side, and the opposite side as the back side.

In Fig. 7, the calculated distributions of the velocity and the static pressure in the midheight plane perpendicular to the turbine axis are represented at six different positions of the turbine. They show the complex interaction that exists between the flow and the turbine, and especially between the jet and the two vanes that are impacted by it. As the turbine rotates, Vane 1 comes into contact with the jet and interferes with Vane 2, which progressively losses the influence of the jet. In this process, the jet accelerates near the tip of Vane 1 at the early positions ($\varphi_T = 12-24$ deg), producing a low-pressure zone at the back side of the vane. In further positions, however, there is a pressure increase in the region between the back side of Vane 1 and the front side of Vane 2 ($\varphi_T = 36-48$ deg). It seems to be produced by the fact that a piece of high-velocity fluid coming from the jet becomes confined within this region and gradually decelerates. The low-pressure vortex that is formed at the front of Vane 1 as a result of the high-shear layer produced between the flow carried by the turbine and the jet sliding across the front side of the vane is also noticeable. The depression related to this vortex has been found to be more important as the flow rate increases.

It is important to note that the pressure difference between the inlet and the outlet of the meter is not constant but varies with the position of the turbine. Figure 8 shows that the pressure difference is the lowest at the initial position considered and has its largest value at 14 deg, approximately. This variable pressure difference is generated, not only by the hydraulic losses but also by the energy interchange that exists between the turbine and the flow in the chamber. Actually, it is the pressure at the inlet, which varies, since the pressure at the outlet has been set constant. This fact explains the variation of the pressure distribution in the inlet pipe observed in Fig. 7. The pressure distribution in the outlet pipe, however, is maintained nearly unchanged apart from the region close to the intersection with the chamber, where it is somewhat influenced by the passing of the vanes. This intersection is quite abrupt and the flow considerably accelerates when it turns to leave the chamber, forming a region with a negative gauge pressure. This depression becomes more significant as the flow rate increases, being as high as -100 kPa relative to the imposed outlet pressure (i.e., zero gauge) in the case of the highest flow rate. Since the outlet pressure would typically be between 500 kPa and 600 kPa in actual working conditions, the possible appearance of cavitation at this point can be dismissed.

The torques exerted by the flow on each of the five vanes of the turbine in a period are illustrated in Fig. 9(*a*). As expected, the only vanes that provided a driving (positive) torque are those impacted by the jet, i.e., Vanes 1 and 2, although it is not the case at their early and late positions, respectively. The remaining three vanes do not come into contact with the jet and they exclusively drag water; hence, they are given only a retarding (negative) torque. It is interesting to point out that it has been verified that

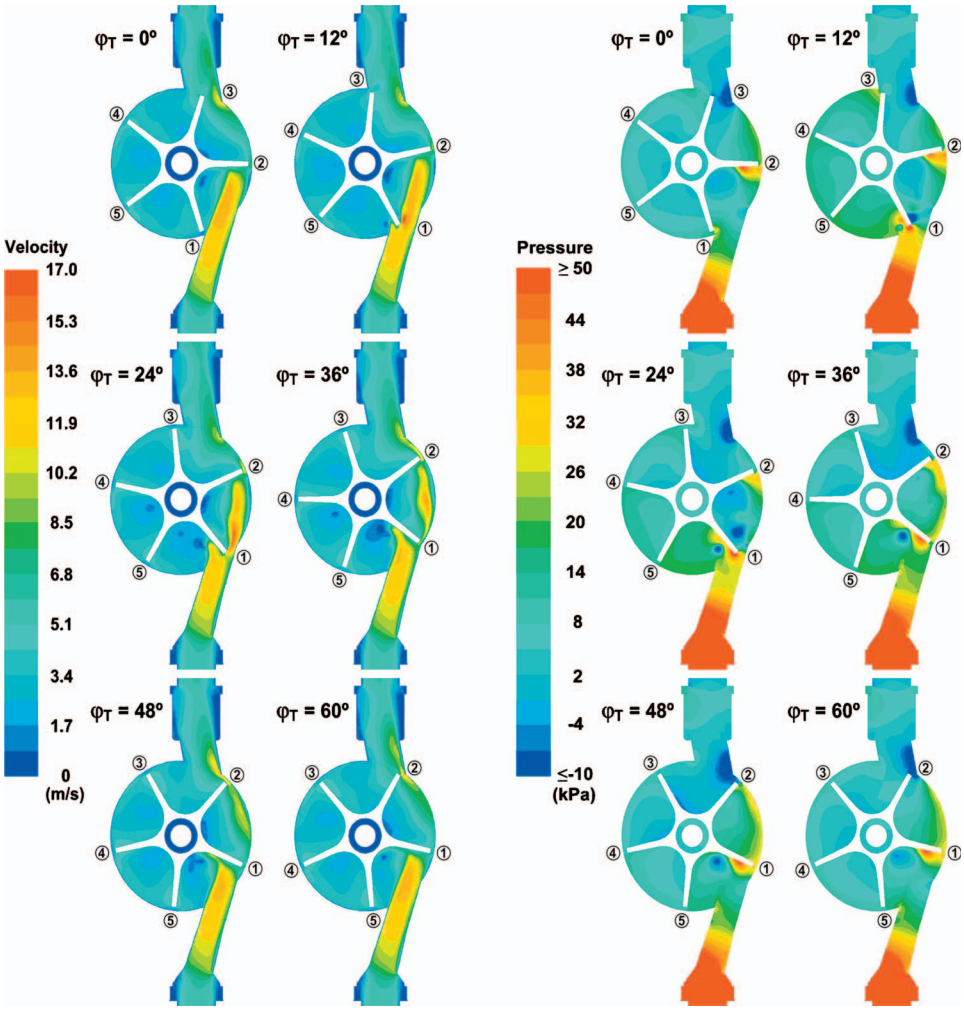

Fig. 7 Detail of the flow with 3000 l/h. Velocity (left) and static pressure (right) in a mid-height plane at different positions of the turbine.

the torques on the five vanes are mainly produced by pressure forces, the shear forces contributing less than 1% at virtually all the positions. The torques imparted to each of the five vanes have been added together to compute the total torque produced by the flow (T_F). This torque is the only one applied upon the turbine in the simulation because the mechanical resistance torque (T_{MR}) has been neglected in this case, as is the case in the remaining simulations of flow rates above 120 l/h. Figure 9(*b*) depicts the variations of the total torque and the rotation speed of the turbine in a period. The sign of the total torque points out whether the sum of the torques on the vanes (and T_{MR} when considered) results in a driving or a retarding torque, and thus whether the turbine accelerates or decelerates. The peak to peak variation of the rotation speed is as much as 20% of its mean value in the period (188 rad/s in this case), as a result of the highly variable torque exerted by the flow and the low inertia moment that the turbine has. Logically, the peaks in rotation speed arise when all the driving and retarding torques applied upon the turbine cancel out and the total torque is zero. Another characteristic of the total torque applied upon the turbine that could be anticipated is that its average in one period is zero. This feature is needed for the turbine's rotation movement to be periodic.

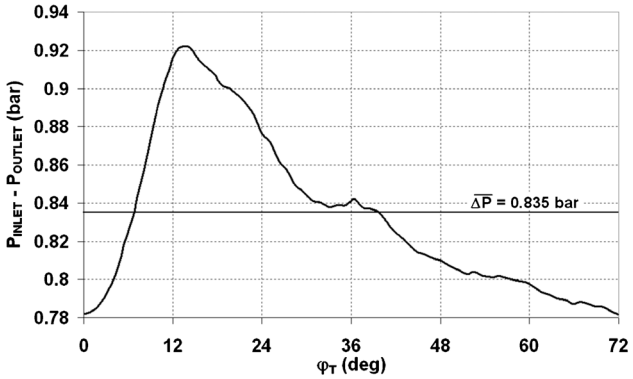

Fig. 8 Static pressure variation between the outlet and the inlet of the meter during a period (Q=3000 l/h)

As is clearly shown in Fig. 9, the computed driving and retarding torques and turbine's rotation speed are far from the assumptions of unchanging torque upon each vane and constant speed of the turbine that are made in the simple analytical model proposed by Chen [2]. In the case of Vanes 3, 4, and 5, the variation of the retarding torque that they receive is related to both the change in the turbine's rotation speed and the proximity of either the inlet or outlet pipes. Apart from the early positions of Vane 3, in which it faces the effects of the flow exiting from the outlet pipe, the retarding torques provided to these three vanes increase with the speed of the turbine and reach the maximum very close to the position at which the rotation speed of the turbine is the highest ($\varphi_T \approx 42$ deg). Moreover, the torques are approximately the same

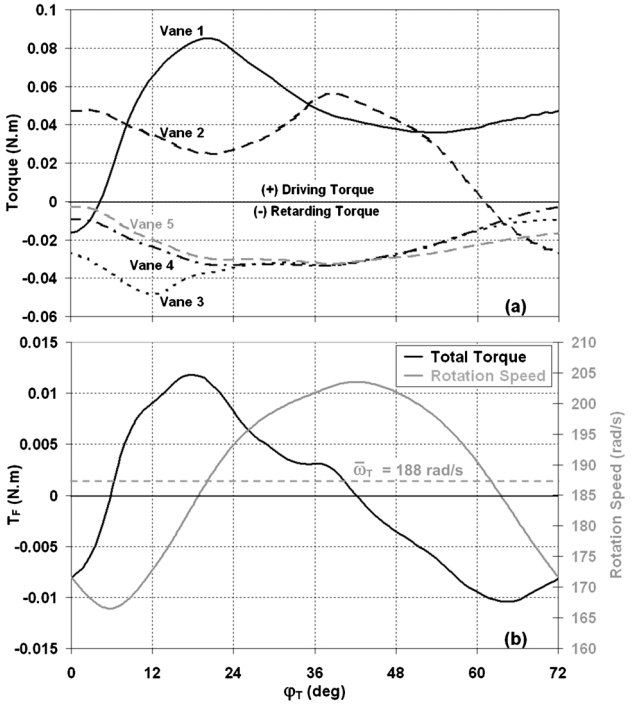

Fig. 9 Periodical turbine-flow interaction (*Q*=3000 l/h): (*a*) torque exerted on each vane and (*b*) total torque and rotation speed of the turbine

in the range φ_T=30–48 deg, in which both Vane 3 and Vane 5 are far from the outlet and inlet pipes, respectively. Out of this range, the effect of the outlet pipe on the torque received by Vane 3 is noticeable, with a significant maximum value at φ_T=12 deg that is produced by a high pressure zone appearing at its back side when it is about to finish passing across the pipe. The effect of the inlet pipe on the torque upon Vane 5 from φ_T=48 deg on is more modest, however, and the torque deviates only moderately from those of Vanes 3 and 4, even when the vane is quite close to the inlet.

The variations of the torques on Vanes 1 and 2 are even more remarkable and clearly depend on the extent in which the vanes are impacted by the jet rather than on the rotation speed of the turbine. At the initial position (φ_T=0 deg), only Vane 2 is impacted by the jet and solely contributes to the driving torque, which is overcome by the retarding torque provided to the rest of the vanes. As the turbine rotates, Vane 1 comes into contact with the jet and quickly starts to contribute to the driving torque. The steep increase of this vane's torque at the early positions is partly produced by the low-pressure zone produced by the accelerated jet at its back side. Although Vane 1 progressively interferes with Vane 2 and reduces its torque, the overall driving torque received by both vanes increases and prevails over the retarding torque, producing the acceleration of the turbine. The total torque has its maximum at a position of φ_T=18 deg approximately, just before the driving torque provided to Vane 1 has its highest value ($\varphi_T \approx$20 deg). Although in subsequent positions this vane takes up a bigger portion of the jet, the pressure at its back side increases and the driving torque that it receives diminishes. Simultaneously, the driving torque produced on Vane 2 recovers and reaches its maximum (at φ_T=40 deg approximately) in spite of the interference of Vane 1 that progressively blocks the jet. This growth is produced because the pressure gradually increases at its front side and diminishes at the back side. Soon after this position, the retarding torque overcomes the driving torque and the turbine starts to slow down. The torque on Vane 2 decreases as this vane get closer to the position of the outlet pipe at φ_T=60 deg, where the influence of the jet is almost completely lost. The torque applied to Vane 1 that has also been decreasing is recovered to some extent at the end of the period, being the only contributor to the driving torque.

The variations of the torques and the rotation speed just discussed are similar in the case of the other flow rates studied, although there are some differences that result in the expected nonlinearity of the water meter's measurements. The comparison between the results obtained with different flow rates has been carried out by means of the dimensionless form of the torque and the rotation speed, which have been defined as

$$\Psi = \frac{T_F}{\rho Q V d} \tag{10}$$

$$\Omega = \frac{\omega_T}{V/d} \tag{11}$$

where V and d are, respectively, the mean velocity of the jet as it enters the chamber and the distance between the axis of the jet and the rotation axis (**k**). Both dimensionless torque and rotation speed have been plotted in Fig. 10 versus the position of the turbine for the ten flow rates studied. The results correspond to simulations in which the friction torque has not been considered, since only the effect of the flow rate is to be investigated. Figure 10(*a*) clearly shows that the dimensionless torque curves of the flow rates in turbulent regime almost coincide, and thus that the torque nearly scales with the square of the flow rate. The same can be stated about the curves that correspond to flow rates in transitional regime (30–120 l/h), as can be seen in Fig. 10(*b*). However, the curves of the flow rates in laminar regime (15 l/h and 22.5 l/h) differ somewhat from the curves corresponding to the other flow regimes. Indeed, they posses higher maxima and have a different form between φ_T=30–48 deg, but almost share with the other curves the positions in which the torque becomes positive ($\varphi_T \approx$6 deg); it has its maximum ($\varphi_T \approx$18 deg), and its minimum ($\varphi_T \approx$67 deg).

The calculated dimensionless mean rotation speed is directly related to the measurement error predicted by the simulation. Actually, the percentage in which the calculated and the expected mean rotation speeds differ is exactly the error made by the meter in the measurement of the water volume that has passed through (see the Appendix):

$$\text{Meas. Error} = \frac{\bar{\Omega}_{\text{calculated}} - \bar{\Omega}_{\text{expected}}}{\bar{\Omega}_{\text{expected}}} \tag{12}$$

Therefore, the nonlinearity of the measurements provided by the meter is clearly shown in Figs. 10(*c*) and 10(*d*), since the difference between the calculated and the expected dimensionless mean rotation speeds varies with the flow rate. The errors in volume measurement corresponding to 3000 l/h and 30 l/h have been indicated in these figures as an example. It is interesting to point out that the way in which the dimensionless rotation speed curves change with the flow rate depends on the flow regime. On the one hand, in turbulent and transitional regimes, the shape of the curve is maintained but the curve itself, in its entirety, shifts up as the flow rate decreases, hence, so does the resultant dimensionless mean rotation speed. The rise, however, is very modest between 60 l/h and 30 l/h and especially between 450 l/h and 300 l/h. On the other hand, in laminar regime, the whole curve does not shift, but only the portion between φ_T=6–60 deg shifts down as the flow rate decreases, so that the dimensionless mean rotation speed diminishes. Certainly, results with more flow rates in laminar regime would be necessary to assess this trend.

6.2 Validation of the Mathematical Model. The mathematical model has been validated by comparing the results of the turbine's mean rotation speed, error in volume measurement, and pressure drop with the experimental measurements obtained in the test rig. The mechanical resistance torque (T_{MR}) has been kept out

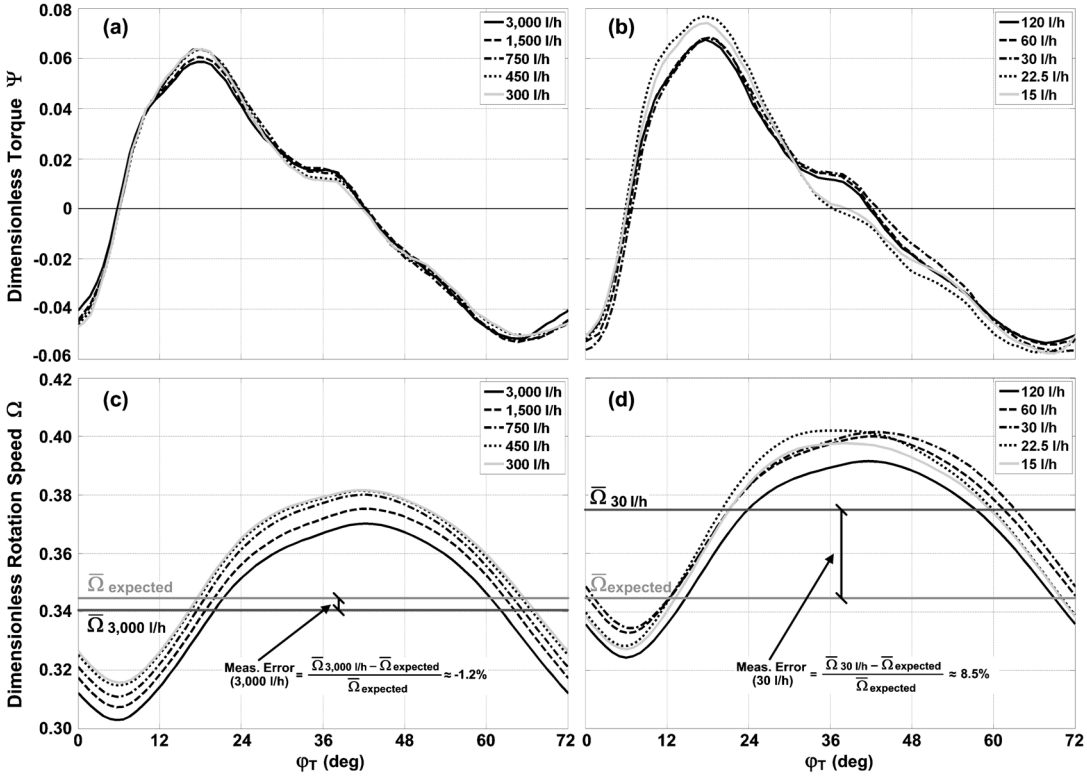

Fig. 10 Dimensionless torque and rotation speed curves with different flow rates: in turbulent regime ((*a*) and (*c*)) and in transitional and laminar regimes ((*b*) and (*d*))

of this validation process because its actual value is not known, so the numerical results compared correspond to simulations in which this torque has not been taken into account. For this reason, the results of low flow rates that are affected by mechanical friction should be expected to differ from those measured.

First, the mean rotation speed of the turbine has been calculated in each simulation by averaging the instantaneous speed throughout one period. The obtained mean rotation speeds are compared to those experimentally measured in Fig. 11. As was expected, they have been found to be approximately proportional to the flow rate. Moreover, the agreement between the calculated and the measured speeds is very good for flow rates higher than 22.5 l/h, the difference being 3% at most (at 3000 l/h). The fact that the discrepancy is small in the case of the three flow rates simulated in transitional regime (30 l/h, 60 l/h, and 120 l/h) confirms that the inability of the turbulence models used here to accurately predict the transition to turbulence has little impact on the capacity of the model to forecast the mean rotation speed of the turbine. The deviation found in the case of the two lowest flow rates is higher, especially for 15 l/h, of which the calculated mean rotation speed is 11% higher than the measured one. Interestingly, the mean speeds calculated with these two flow rates are higher than the measured ones, as is the case of 30 l/h and 60 l/h. It is consistent with the fact that mechanical friction, which tends to slow the turbine down, has not been taken into account. In the study about the effect of the friction presented below, it will be confirmed that these calculated speeds get closer to the measured ones when friction is considered.

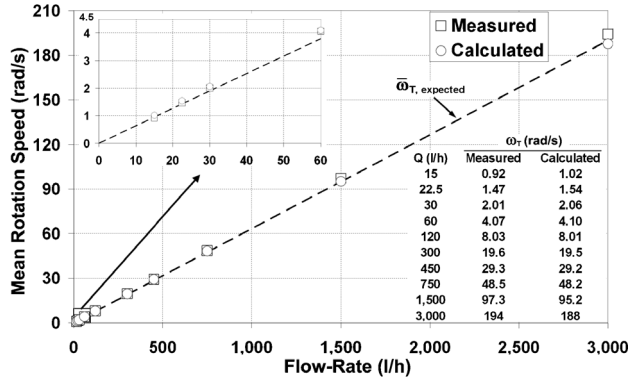

Fig. 11 Mean rotation speed of the turbine. Measured versus calculated values.

As discussed above, the pressure drop produced in the meter is not constant in the simulations, but depends on the position of the turbine. The mean pressure drop has been calculated for the flow rates between 450 l/h and 3000 l/h by averaging its value throughout one period. The predictions are in very good agreement with experimental measurements, as is depicted in Fig. 12. Both experimental and numerical results evidence a nearly quadratic variation with the flow rate observed in many references [1].

Finally, the error curve predicted by the mathematical model has been compared to the curve experimentally obtained. Both curves are plotted together in Fig. 13, where the accuracy requirements of the ISO 4064 standard [29] are indicated. The fact that some values of the measurement error do not conform to these requirements is of no importance since the meter studied is a noncommercial prototype. The measurement errors appearing in the calculated error curve have been computed comparing the calculated and the expected dimensionless mean rotation speeds, as was explained above. Therefore, the calculated error curve evidences the different trends that the turbine's dimensionless mean rotation speed exhibits with different flow regimes.

As is shown in Fig. 13, the mathematical model very accurately reproduces the shape of the experimental error curve in the range between 120 l/h and 750 l/h, but deviates from it at lower and

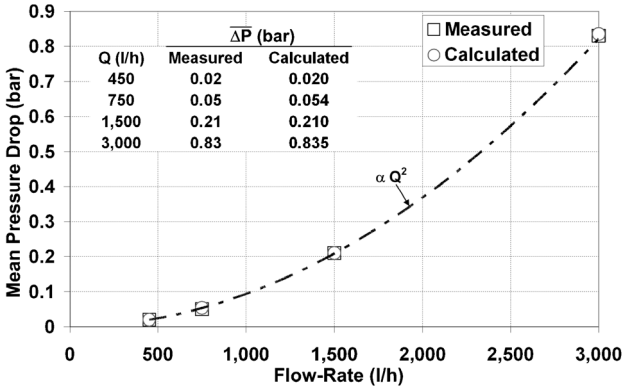

Fig. 12 Mean pressure drop. Measured versus calculated values.

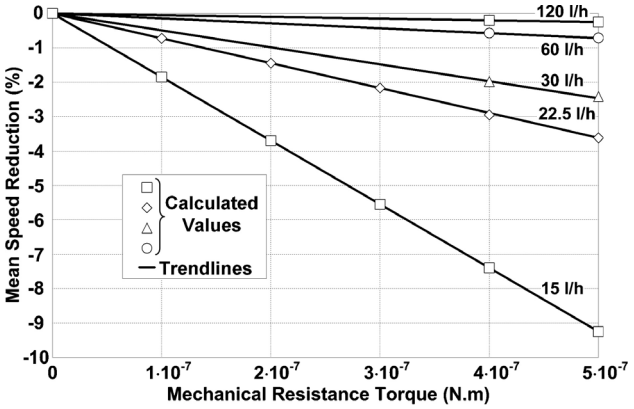

Fig. 14 Reduction in the mean speed of the turbine as a function of mechanical resistance torque (T_{MR})

higher flow rates. The deviation to more positive errors (i.e., more volume registered) observed in the case of lower flow rates is consistent with the fact that mechanical friction has not been considered. Actually, in the next section, the mathematical model will be shown capable of reproducing the steep decline observed in the experimental curve when mechanical friction is included.

With regard to the highest flow rates, namely, 1500 l/h and 3000 l/h, the deviation from the measurements might be due to the combination of two causes. On the one hand, the computational mesh is probably not fine enough to accurately calculate the thinner boundary layers found in such high flow rates. The higher discretization error calculated in these simulations and the fact that large values of y^+ (up to 30) exist at some wall-adjacent cell zones would confirm this point. On the other hand, the rotation speed of the turbine may be so important at these high flow rates that the centrifugal forces to which the flow is subjected in the chamber might have a significant impact on turbulence. The turbulence models based on the Boussinesq hypothesis, such as the ones employed in this study, are incapable of reproducing the anisotropy of the Reynolds stresses caused by this phenomenon and the result that this anisotropy has on the flow [9]. Therefore, some differences between the calculated and the actual flows and, ultimately, between the calculated and the experimental measurement errors may be expected if the mentioned rotation effects are significant. Nevertheless, these differences seem to be minor in light of the comparison between the calculated and the measured values.

6.3 Study of the Effect of Mechanical Friction on Meter Performance. The results presented thus far correspond to simulations in which the retarding torque due to the mechanical friction (T_{MR}) has not been considered. The discrepancies found in the lower part of the measuring range between the experimental and the simulated mean rotation speed and measurement error were thus anticipated, because the magnitude of the ignored mechanical resistance torque (T_{MR}) is likely to be similar to that produced by the flow (T_F) at such a low flow rates. However, the performance of the water meter in the lower part of the measuring range is very important to the designers, since this performance is related to sensitivity, that being the water meter's capability of providing a measure at low flow rates with a margin of error that meets legal requirements. Consequently, the effect of mechanical friction on the turbine's mean rotation speed and the meter's error curve has been analyzed using the mathematical model developed.

The main difficulty in undertaking this analysis is to determine the mechanical resistance torque whether it be experimentally or theoretically. In the present study, however, its magnitude has been estimated as being of the order of 10^{-7} N m from the values of T_F calculated in the simulations with 15 l/h and 22.5 l/h when the friction is not regarded. Moreover, its possible dependence on the turbine's speed has been neglected in such a way that its value has been considered constant in each simulation. These two assumptions are based on the fact that the importance of the flow and the mechanical friction on the meter's performance is similar at low flow rates.

In this study, the mathematical model has been simulated with flow rates between 15 l/h and 120 l/h using different values for the mechanical resistance torque (T_{MR}) up to 5×10^{-7} N m. The values of the turbine's mean rotation speed obtained from these simulations are, obviously, smaller than those obtained when the mechanical resistance torque was not factored in. However, a remarkable result is obtained when the values of the reduction of mean rotation speed are plotted against the values of T_{MR} for a constant value of the flow rate, as has been done in Fig. 14. Interestingly, the reduction of the mean rotation speed is found to be proportional to the value of T_{MR} in which the constant of proportionality is a function of the flow rate. Moreover, the effect of a given constant value of the resistance torque on the mean speed of the turbine notably decreases as the flow rate increases. This trend was expected since T_F is nearly scaled with the square of the flow rate (see Fig. 10) and quickly overcomes the friction torque as the flow rate is increased. Indeed, the speed reduction produced with 120 l/h is very small and it can be predicted to be negligible in the case of higher flow rates. This result is in agreement with the experiments of Arregui et al. [17] that carried out accelerated wear tests on several single-jet water meters of the same size and measuring range of that studied in this work and concluded that the effect of the augmented mechanical friction was only noticeable with flow rates of 120 l/h and below.

Another interesting result is shown when the error curves obtained from the mathematical model considering mechanical fric-

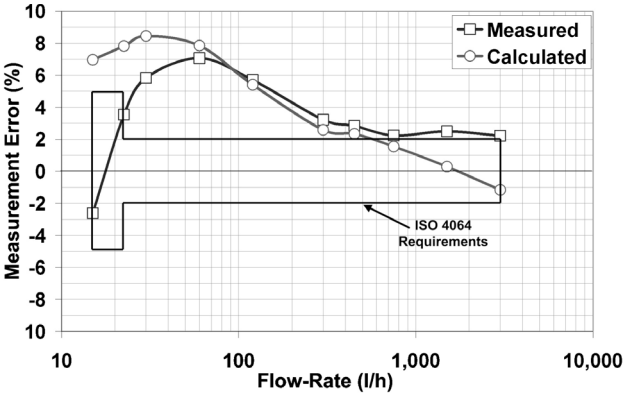

Fig. 13 Error curve. Measured versus calculated values.

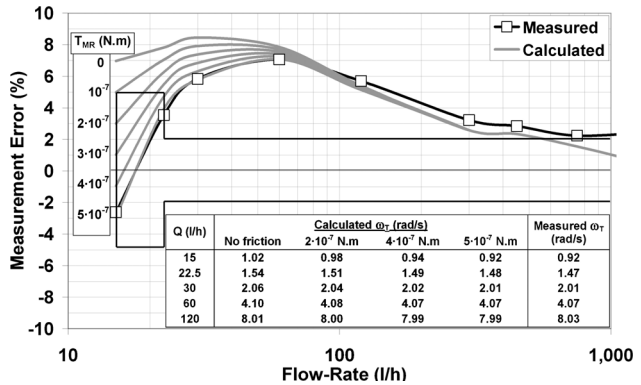

Q (l/h)	Calculated ω_T (rad/s) No friction	$2{\cdot}10^{-7}$ N.m	$4{\cdot}10^{-7}$ N.m	$5{\cdot}10^{-7}$ N.m	Measured ω_T (rad/s)
15	1.02	0.98	0.94	0.92	0.92
22.5	1.54	1.51	1.49	1.48	1.47
30	2.06	2.04	2.02	2.01	2.01
60	4.10	4.08	4.07	4.07	4.07
120	8.01	8.00	7.99	7.99	8.03

Fig. 15 Comparison between experimental and calculated values of measurement error and mean rotation speed with different mechanical resistance torques (T_{MR})

tion are represented. Figure 15 shows the change experienced by the calculated error curve when different constant values of the mechanical resistance torque are considered. The speed reduction produced by this torque implies that less water volume is registered by the meter and therefore makes the measurement error approach, or penetrate deeper into, the negative region. As the value of the torque increases, the calculated error curve tends to reproduce the steep decline observed in the experimental curve and even matches with the latter at a value of 5×10^{-7} N m. These results seem to confirm the initial hypotheses about the magnitude of the mechanical resistance torque and its invariability with the rotation speed of the turbine.

Furthermore, the results obtained in this study could be used by the designers to quantify the effect that a reduction of the mechanical friction would have in the lower part of the error curve. For example, if the related torque is reduced from 5×10^{-7} N m to 2×10^{-7} N m, the measurement error at 15 l/h changes from −3% to +3% and the decline of the error curve is notably minimized.

7 Conclusions

The mathematical model developed has allowed a detailed analysis of the performance of a single-jet water meter to be carried out within a wide measuring range, which expanded from 15 l/h to 3000 l/h and included flow rates in laminar, transitional, and turbulent flow regimes. For this end, the simulations of the three dimensional flow within the meter have followed a devised time-marching procedure to resolve the interaction between the flow and the turbine, thus providing the position and the rotation speed as part of the solution. This feature allowed analyzing the error curve of the meter, hence assessing its behavior as a measuring device.

Moreover, the detailed information provided by the simulations made it possible to thoroughly analyze the interaction between the flow and the turbine. This interaction has proven to be very complex since it comprehends the combined effects of the action of the jet over two vanes, the resistance over the remaining vanes that drag water, and the flow exiting from the outlet pipe. The resulting torques exerted by the flow and variable speed of the turbine have been analyzed in detail and have revealed the difficulty of modeling the performance of a single-jet water meter with a simple analytical model. Additionally, the dimensionless torque and rotation speed curves have been presented for different flow rates. In the case of the water meter studied, the changes in these curves as the flow rate varies show different trends depending on the flow regime. The different trends found in the dimensionless rotation speed are directly related to the form of the error curve obtained from the mathematical model.

Three units of the analyzed water meter design have been built and tested in an experimental test rig to validate the mathematical model when the torque produced by the mechanical friction upon the turbine is not considered. The simulated mean values of pressure drop and the turbine's rotation speed have been compared to those experimentally obtained and have been found to be in good agreement. Moreover, the error curve obtained from the mathematical model accurately reproduced the values and the trend of the experimental curve in the range between 120 l/h and 750 l/h, although deviated from it at lower and higher flow rates. These divergences came from different sources. At higher flow rates, the deviation could be related to an insufficient mesh resolution and to the inability of the turbulence model to reproduce the effect of rotation on turbulence. The deviation found at lower flow rates came precisely from the fact that the torque produced by the mechanical friction had been ignored.

When the torque produced by the mechanical friction is taken into account, the trend of the experimental error curve at low flow rates is correctly reproduced by that obtained from the mathematical model. This result has been obtained by undertaking a study in which different constant values of the retarding torque due to the friction have been included in the mathematical model. This study has led to two important conclusions. First, the mean rotation speed of the turbine linearly decreases along the estimated retarding torque value range. Second, it has been confirmed that the effect of mechanical friction is only noticeable at low flow rates (up to 120 l/h in this case). Finally, the study has shown to be valuable for quantifying the effect that an improvement in the mechanical friction would have on the error curve.

To sum up, the present study shows that mathematical modeling and simulation using CFD techniques is a valuable tool for the design of single-jet water meters, even more so if one considers the difficulty of developing a simplified model of their performance and the cost of extracting useful information from the experiments. The encouraging results of this study have led to the application of the proposed methodology in the identification of the most important and influential design parameters, and finally, to produce an optimum design.

Acknowledgment

This research was carried out with the support of ELSTER Iberconta S.A. and was partially funded by Ministerio de Educación y Ciencia (Spain) through the Programa PROFIT, CIT-020600-2005-023 and by Eusko Jaurlaritza-Gobierno Vasco (Spain) through the Programa SAIOTEK, MERIV002. The authors would like to thank José Bernardo de la Quintana, Jesús Urraca, and David Fuentes for their valuable help. The financial support of Cátedra Fundación Antonio Aranzábal–Universidad de Navarra is gratefully acknowledged.

Appendix: Relation Between the Mean Rotation Speed of the Turbine and Measurement Error

In the simulations, the error in volume measurement might be calculated as the difference that exists in each period between the actual volume delivered (V_{actual}) and the volume registered by the meter (V_{regist}).

$$\text{Meas. Error} = \frac{V_{\text{regist.}} - V_{\text{actual}}}{V_{\text{actual}}} \tag{A1}$$

However, these volumes are directly related to the calculated and expected turbine's mean rotation speeds, so that the measurement error can be calculated from these values. The relations are shown below.

(1) The actual volume delivered (V_{actual}) equals the time period T times the flow rate established in the simulation.

$$V_{\text{actual}} = TQ \tag{A2}$$

Moreover, the calculated mean rotation speed is related to the time period as

$$T = \frac{2\pi/5}{\bar{\omega}_{T,\text{calc.}}} \tag{A3}$$

Combining Eqs. (A2) and (A3), the relation between the actual volume delivered and the calculated mean rotation speed is found to be

$$V_{\text{actual}} = \frac{2\pi/5}{\bar{\omega}_{T,\text{calc.}}} Q \tag{A4}$$

(2) The volume registered in a period (V_{regist}) is one-fifth of the volume registered in one revolution of the turbine.

$$V_{\text{regist.}} = \frac{1}{5} K^{-1} \tag{A5}$$

Additionally, the expected mean rotation speed is related to the meter factor K as

$$\bar{\omega}_{T,\text{expected}} = 2\pi K Q \tag{A6}$$

Combining Eqs. (A5) and (A6), the relation between the registered volume and the expected mean rotation speed is found to be

$$V_{\text{regist.}} = \frac{2\pi/5}{\bar{\omega}_{T,\text{expected}}} Q \tag{A7}$$

Finally, substitution of Eqs. (A4) and (A7) into Eq. (A1) yields the expression of the measurement error that has been used in the study:

$$\text{Meas. Error} = \frac{\bar{\omega}_{T,\text{calculated}} - \bar{\omega}_{T,\text{expected}}}{\bar{\omega}_{T,\text{expected}}} = \frac{\bar{\Omega}_{\text{calculated}} - \bar{\Omega}_{\text{expected}}}{\bar{\Omega}_{\text{expected}}} \tag{A8}$$

References

[1] Meinecke, W., 1984, "Measuring Characteristics of Water Meters," Aqua, **4**, pp. 233–237.

[2] Chen, J. S. J., 2000, "On the Design of a Wide Range Mini-flow Paddlewheel Flow Sensor," Sens. Actuators, A, **87**, pp. 1–10.

[3] Buckle, U., Durst, F., Howe, B., and Melling, A., 1992, "Investigation of a Floating Element Flowmeter," Flow Meas. Instrum., **3**, pp. 215–225.

[4] Buckle, U., Durst, F., Kochner, H., and Melling, A., 1995, "Further Investigation of a Floating Element Flowmeter," Flow Meas. Instrum., **6**, pp. 75–78.

[5] Xu, Y., 1992, "Calculation of the Flow Around Turbine Flowmeter Blades," Flow Meas. Instrum., **3**, pp. 25–35.

[6] Xu, Y., 1992, "A Model for the Prediction of Turbine Flowmeter Performance," Flow Meas. Instrum., **3**, pp. 37–43.

[7] Abouri, D., Parry, A., and Hamdouni, A., 2004, "A Stable Fluid Rigid Body Interaction Algorithm: Application to Industrial Problems," *2004 ASME/ISME Pressure Vessels and Piping Conference*, San Diego, CA.

[8] Sánchez, G., and Rivas, A., 2003, "Computational Fluid Dynamics Approach to the Design of a Single-Jet Water-Meter," *Pumps, Electromechanical Devices and Systems Applied to Urban Water Management*, E. Cabrera and E. Cabrera, Jr., eds., Balkema, Lisse, The Netherlands, Vol. 2, pp. 405–413.

[9] Wilcox, D. C., 1998, *Turbulence Modeling for CFD*, DCW Industries, La Canada, CA.

[10] Chen, H. C., and Patel, V. C., 1988, "Near-Wall Turbulence Models for Complex Flows Including Separation," AIAA J., **26**(6), pp. 641–648.

[11] Shih, T.-H., Liou, W. W., Shabbir, A., Yang, Z., and Zhu, J., 1995, "New k-ε Eddy Viscosity Model for High Reynolds Number Turbulents Flows," Comput. Fluids, **24**, pp. 227–238.

[12] Wolfshtein, M., 1969, "The Velocity and Temperature Distribution of One-Dimensional Flow With Turbulence Augmentation and Pressure Gradient," Int. J. Heat Mass Transfer, **12**, pp. 301–318.

[13] Jongen, T., and Marx, Y. P., 1997, "Design of an Unconditionally Stable, Positive Scheme for the k-ε and Two-Layer Turbulence Models," Comput. Fluids, **26**(5), pp. 469–487.

[14] Suzen, Y. B., and Huang, P. G., 2000, "Modeling of Flow Transition Using an Intermittency Transport Equation," ASME J. Fluids Eng., **122**(2), pp. 273–284.

[15] Menter, F. R., Langtry, R. B., Likki, S. R., Suzen, Y. B., Huang, P. G., and Volker, S., 2006, "A Correlation-Based Transition Model Using Local Variables—Part I: Model Formulation," ASME J. Turbomach., **128**(3), pp. 413–422.

[16] Rodi, W., 1991, "Experience With Two-layer Models Combining the k-ε Model With a One-equation Model Near the Wall," AIAA Paper No. 91-0216.

[17] Arregui, F., Cabrera, E. J., Cobacho, R., and García-Serra, J., 2005, "Key Factors Affecting Water Meter Accuracy," Leakage 2005, Halifax, Canada.

[18] Murthy, J. Y., and Mathur, S. R., 1997, "Periodic Flow and Heat Transfer Using Unstructured Meshes," Int. J. Numer. Methods Fluids, **25**, pp. 659–677.

[19] Patankar, S. V., 1980, *Numerical Heat Transfer and Fluid Flow*, Hemisphere, New York.

[20] Barth, T. J., and Jespersen, D., 1989, "The Design and Application of Upwind Schemes on Unstructured Meshes," AIAA Paper No. 89-0366.

[21] Mathur, S., and Murthy, J. Y., 1997, "A Pressure-Based Method for Unstructured Meshes," Numer. Heat Transfer, Part B, **31**(2), pp. 195–215.

[22] Vandoormaal, J. P., and Raithby, G. D., 1984, "Enhancements of the SIMPLE Method for Predicting Incompressible Fluid Flows," Numer. Heat Transfer, **7**, pp. 147–163.

[23] Rhie, C. M., and Chow, W. L., 1983, "Numerical Study of the Turbulent Flow Past an Airfoil With Trailing Edge Separation," AIAA J., **21**(11), pp. 1525–1532.

[24] Mathur, S. R., 1994, "Unsteady Flow Simulations Using Unstructured Sliding Meshes," AIAA Paper No. 94-2333.

[25] Benra, F. K., 2006, "Numerical and Experimental Investigation on the Flow Induced Oscillations of a Single-Blade Pump Impeller," ASME J. Fluids Eng., **128**(4), pp. 783–793.

[26] Le Tallec, P., and Mouro, J., 2001, "Fluid Structure Interaction with Large Structural Displacements," Comput. Methods Appl. Mech. Eng., **190**, pp. 3039–3067.

[27] Celik, I., and Karatekin, O., 1997, "Numerical Experiments on Application of Richardson Extrapolation With Nonuniform Grids," ASME J. Fluids Eng., **119**, pp. 584–590.

[28] White, F. M., 2007, *Fluid Mechanics*, McGraw-Hill, New York.

[29] ISO 4064-1:2005, "Measurement of Water Flow in Fully Charged Closed Conduits—Meters for Cold Potable Water and Hot Water—Part 1: Specifications."